Investigating the relationship between thalamic iron concentration and disease severity in secondary progressive multiple sclerosis using quantitative susceptibility mapping: Cross-sectional analysis from the MS-STAT2 randomised controlled trial

Thomas Williams [a,*], Nevin John [a,b], Alberto Calvi [a], Alessia Bianchi [a], Floriana De Angelis [a], Anisha Doshi [a], Sarah Wright [a], Madiha Shatila [a], Marios C. Yiannakas [a], Fatima Chowdhury [a], Jon Stutters [a], Antonio Ricciardi [a], Ferran Prados [a,c,d], David MacManus [a], Francesco Grussu [a,c], Anita Karsa [i], Becky Samson [a,c], Marco Battiston [a,c], Claudia A.M. Gandini Wheeler-Kingshott [a,g], Karin Shmueli [i], Olga Ciccarelli [a,f], Frederik Barkhof [a,c,f,h], Jeremy Chataway [a,e,f], On behalf ofThe UCL MS-STAT2 investigators[2]

[a] NMR Research Unit, Queen Square Multiple Sclerosis Centre, Department of Neuroinflammation, UCL Queen Square Institute of Neurology, Faculty of Brain Sciences, University College London, London, United Kingdom
[b] Monash University, Department of Medicine, School of Clinical Sciences, Clayton, Australia
[c] University College London, Centre for Medical Image Computing, Department of Medical Physics and Biomedical Engineering, London, United Kingdom
[d] Universitat Oberta de Catalunya, Barcelona, Spain
[e] Medical Research Council Clinical Trials Unit at UCL, Institute of Clinical Trials and Methodology, United Kingdom
[f] National Institute for Health Research, Biomedical Research Centre, University College London Hospitals, London, United Kingdom
[g] Department of Brain and Behavioural Sciences, University of Pavia, Pavia, Italy
[h] Vrije Universiteit Amsterdam, Department of Radiology & Nuclear Medicine, VU University Medical Centre, Amsterdam, Netherlands
[i] Department of Medical Physics and Biomedical Engineering, University College London, London, United Kingdom

ARTICLE INFO

ABSTRACT

Background: Deep grey matter pathology is a key driver of disability worsening in people with multiple sclerosis. Quantitative susceptibility mapping (QSM) is an advanced magnetic resonance imaging (MRI) technique which quantifies local magnetic susceptibility from variations in phase produced by changes in the local magnetic field. In the deep grey matter, susceptibility has previously been validated against tissue iron concentration. However, it currently remains unknown whether susceptibility is abnormal in older progressive MS cohorts, and whether it correlates with disability.

Objectives: To investigate differences in mean regional susceptibility in deep grey matter between people with secondary progressive multiple sclerosis (SPMS) and healthy controls; to examine in patients the relationships between deep grey matter susceptibility and clinical and imaging measures of disease severity.

Methods: Baseline data from a subgroup of the MS-STAT2 trial (simvastatin vs. placebo in SPMS, NCT03387670) were included. The subgroup underwent clinical assessments and an advanced MRI protocol at 3T. A cohort of age-matched healthy controls underwent the same MRI protocol. Susceptibility maps were reconstructed using a robust QSM pipeline from multi-echo 3D gradient-echo sequence. Regions of interest (ROIs) in the thalamus, globus pallidus and putamen were segmented from 3D T1-weighted images, and lesions segmented from 3D fluid-attenuated inversion recovery images. Linear regression was used to compare susceptibility from ROIs between patients and controls, adjusting for age and sex. Where significant differences were found, we further examined the associations between ROI susceptibility and clinical and imaging measures of MS severity.

Results: 149 SPMS (77% female; mean age: 53 yrs; median Expanded Disability Status Scale (EDSS): 6.0 [interquartile range 4.5–6.0]) and 33 controls (52% female, mean age: 57) were included.

Thalamic susceptibility was significantly lower in SPMS compared to controls: mean (SD) 28.6 (12.8) parts per billion (ppb) in SPMS vs. 39.2 (12.7) ppb in controls; regression coefficient: −12.0 [95% confidence interval: −17.0 to −7.1], $p < 0.001$. In contrast, globus pallidus and putamen susceptibility were similar between both groups.

In SPMS, a 10 ppb lower thalamic susceptibility was associated with a +0.13 [+0.01 to +0.24] point higher EDSS ($p < 0.05$), a −2.4 [−3.8 to −1.0] point lower symbol digit modality test (SDMT, $p = 0.001$), and a −2.4 [−3.7 to −1.1] point lower Sloan low contrast acuity, 2.5% ($p < 0.01$).

Lower thalamic susceptibility was also strongly associated with a higher T2 lesion volume (T2LV, $p < 0.001$) and lower normalised whole brain, deep grey matter and thalamic volumes (all $p < 0.001$).

Conclusions: The reduced thalamic susceptibility found in SPMS compared to controls suggests that thalamic iron concentrations are lower at this advanced stage of the disease. The observed relationships between lower thalamic susceptibility and more severe physical, cognitive and visual disability suggests that reductions in thalamic iron may correlate with important mechanisms of clinical disease progression. Such mechanisms appear to intimately link reductions in thalamic iron with higher T2LV and the development of thalamic atrophy, encouraging further research into QSM-derived thalamic susceptibility as a biomarker of disease severity in SPMS.

1. Introduction

Progressive multiple sclerosis (MS) is characterised by gradually worsening physical and cognitive disability. Standard lesional and volumetric magnetic resonance imaging (MRI) demonstrate that this deterioration is accompanied by an increase in T2-lesion volume (T2LV) and a reduction in brain and spinal cord volumes (Sastre-Garriga et al., 2020).

Aberrant iron homeostasis is increasingly recognised as a potentially important contributor to the neurodegenerative processes in MS (Yong and Yong, 2022). In healthy controls, central nervous system (CNS) iron is typically stored as ferritin within oligodendrocytes, with the highest iron concentrations found within the basal ganglia (Todorich et al., 2009). CNS iron concentrations increase as part of normal aging – rapidly within the first 3 decades, then more slowly thereafter. The thalamus displays unique iron characteristics compared to the other deep grey matter structures: the overall concentration is lower compared to the basal ganglia, and whilst thalamic iron also increases during the first 3 decades, it then subsequently decreases as part of ongoing normal aging (Hallgren and Sourander, 1958).

In people with MS, whilst histological studies have reported similar overall concentrations and regional distributions of CNS iron compared to controls, a number of differences are noted (Haider et al., 2014; Sun et al., 2015). Age-related increases in iron, seen in both control white matter and the basal ganglia, are not observed in MS (Haider et al., 2014; Hametner et al., 2013). Focal demyelinating lesions, whether within white matter or deep grey matter, also modulate local iron concentrations via two main processes. Firstly, loss of oligodendrocytes, as seen in peri-lesional normal appearing white matter or in the centre of chronic inactive lesions, is associated with lower iron concentrations. Conversely, the presence of microglia/macrophages within acutely demyelinating lesions, or at the border of chronic active lesions, is associated with increased iron concentrations (Hametner et al., 2013; Popescu et al., 2017; Tham et al., 2020; Mehta et al., 2013). The balance between oligodendrocyte loss and the presence of microglia/macrophages therefore appears to represent an important contributor to local iron concentrations in MS.

Uncomplexed iron is a potent generator of oxygen free-radicals, perpetuating oxidative stress and mitochondrial dysfunction (Yong and Yong, 2022; Hallgren and Sourander, 1958; Bulters et al., 2018). In support of a potentially pathogenic role of iron in MS, transcriptional profiling suggests that peri-lesional oligodendrocytes actively export iron, and various markers of oxidative stress (axonal spheroids, reactive oligodendrocytes, microglial activation) have been spatially associated with higher iron concentrations (Haider et al., 2014; Hametner et al., 2013).

Susceptibility-based MRI techniques have facilitated the *in vivo* detection of CNS iron. Quantitative susceptibility mapping (QSM), an advanced MRI technique, quantifies local magnetic susceptibility (χ) from variations in phase produced by changes in the local magnetic field (Shmueli et al., 2009). It is therefore sensitive to both iron and myelin, and less influenced by the non-localised field effects and orientation dependence seen with other susceptibility-based techniques (Shmueli et al., 2009). Particularly in the deep grey matter, where the influence of myelin is reduced, higher QSM-derived χ has been validated as an accurate measure of higher CNS iron concentrations (Sun et al., 2015; Langkammer et al., 2012; Hametner et al., 2018; Stüber et al., 2014).

When studied in mixed cohorts of predominantly relapsing remitting MS (RRMS, 65–82%), QSM has been used to demonstrate that *basal ganglia* χ is higher compared to controls, and associated with greater physical disability on the expanded disability status scale (EDSS) (Hagemeier et al., 2018a, 2018b; Zivadinov et al., 2018; Voon et al., 2024). In contrast, the inverse is seen with the *thalamus* – where χ is lower in MS compared to controls, and lower χ associated with more severe disability (Hagemeier et al., 2018a, 2018b; Zivadinov et al., 2018; Voon et al., 2024; Schweser et al., 2018). In longitudinal studies, increasing basal ganglia χ appears to be initiated early in the course of MS, and χ changes are closely associated with changes in structural volumes (Hagemeier et al., 2018b). The basis for the opposing relationships – higher basal ganglia χ, but lower thalamic χ, being associated with MS diagnosis and severity – may relate to regional differences in disease processes. In the basal ganglia, it has been suggested that increased χ may mainly reflect an increased concentration of iron occurring secondary to a reduced structural volume, without increases in the actual iron content (Hagemeier et al., 2018c; Schweser et al., 2020). In contrast, reduced thalamic χ may represent a reduction in the actual iron content secondary to the pathological loss of iron-containing structures (Hagemeier et al., 2018b; Schweser et al., 2018, 2020).

To date, no studies have focused specifically on deep grey matter χ from patients in the more advanced, secondary progressive phase of MS. As discussed above, aging has an established role in normal brain iron accumulation, and previous reports have suggested differences in regional χ between early and late stages of MS (Todorich et al., 2009; Zivadinov et al., 2018; Schweser et al., 2018). Our aims here were therefore to investigate deep grey matter regional χ in an older untreated SPMS cohort, examining differences between patients and controls, and the relationship between deep grey matter χ and other clinical and imaging measures of disease severity.

2. Methods

2.1. Subjects

Participants included in this analysis were all recruited into the MS-STAT2 randomised controlled trial (NCT03387670) at the lead University College London (UCL) site (the only site at which the MRI substudy took place). All participants gave written informed consent; MS-STAT2 was approved by the National Health Service (NHS) national research ethics committee (London - Westminster Research Ethics Committee, October 09, 2017, ref: 17/LO/1509) and all research was carried out according to the Declaration of Helsinki. (World Medical Association).

MS-STAT2 is an ongoing multicentre, interventional phase 3 randomised controlled trial assessing high-dose (80 mg/day) simvastatin versus placebo as a treatment for slowing the progression of disability in patients with SPMS (pwSPMS). Briefly, eligible participants are 25–65 years of age with EDSS 4.0–6.5, with a confirmed diagnosis of SPMS and evidence of ongoing disability progression. The main exclusion criteria were the ongoing use of immunosuppressive disease modifying therapies (with the exception of siponimod) or current use of a statin.

A cohort of healthy controls were similarly recruited. Controls were eligible if they had no known neurological disease, no contraindications to MRI, were of a similar age to that of patients, and were not taking a statin.

2.2. Baseline assessments

Clinical assessments were performed by trained neurologists, and included EDSS, timed 25-foot walk (25FW), timed 9-hole peg test (9HPT), symbol digit modalities test (SDMT), California verbal learning test (CVLT-II), brief visuospatial memory test, revised (BVMT-R) and Sloan low contrast visual acuity (SLCVA).

2.3. MRI

UCL MS-STAT2 participants were offered enrolment into an optional MRI substudy. Consenting participants were all imaged on a Philips Ingenia CX MR system and the product 32 channel head coil. The MRI protocol included a multi-echo 3D sagittal spoiled gradient-echo with 8 echoes (echo time (TE)1/ΔTE = 2.3/3.3 ms, repetition time (TR) = 28.5 ms, flip angle = 24°, 1x1x1 mm^3 resolution), used for QSM analysis; 3D sagittal T1-weighted (3DT1w) magnetisation-prepared turbo field echo (TFE) (TE = 3.2 ms, TR = 6.9 ms, flip angle = 8°, 1x1x1mm^3 resolution), used for tissue segmentations; 3D sagittal fluid-attenuated inversion recovery (FLAIR) (TE = 263 ms, TR = 4800 ms, inversion delay time = 1650 ms, flip angle = 90°, 1x1x1 mm^3 resolution), used for lesion segmentation.

Regions of interest (ROIs) for bilateral thalami, putamen and globus pallidus were segmented using Geodesic Information Flows (GIF) from 3D T1 images (Cardoso et al., 2015). Left and right structural regional volumes were summed to give total volumes for each ROI. Volumes were normalised through the inclusion of estimated total intracranial volume (eTIV) in all relevant regression models (FreeSurfer, 2021; Buckner et al., 2004). Lesions were segmented from 3D FLAIR using NicMSlesions (Valverde et al., 2019).

2.4. QSM processing

The QSM processing pipeline used to generate χ data in this study was optimised using the pipeline in (Karsa et al., 2020) as a starting point. Briefly, non-linear field fitting was used across the first 7 echoes, followed by residual Laplacian phase unwrapping (Liu et al., 2013; Cornell MRI Research Lab, 2020). The final 8th echo was excluded as this reduced the degree of echo-to-echo phase inconsistency whilst maintaining imaging quality (Ricciardi et al., 2021). Background fields were removed using the Projection onto Dipole Fields approach (Liu et al., 2011). The local fields were then used to calculate χ, expressed in parts per billion (ppb) through iterative fitting with Tikhonov regularisation (software available at https://xip.uclb.com/product/mri_qsm_tkd) with correction for susceptibility underestimation (Valverde et al., 2019). This approach has been shown to generate reproducible tissue χ values (Karsa et al., 2020; Schweser et al., 2013; Kiersnowski et al., 2023; Murdoch et al., 2022). Comparisons of various QSM pipelines have previously shown that such iterative fitting approaches are amongst the most accurate (Bilgic et al., 2021). As in previous publications using this pipeline, susceptibility maps were not explicitly referenced to any particular tissue, but were implicitly referenced to the average susceptibility across each image volume (Karsa et al., 2020). ROI χ were determined via GIF parcellations, and as left and right ROI χ did not significantly differ (T-tests, p-values all >0.05), the average between the two was taken to represent bilateral ROI χ. All QSM images were visually inspected for quality and excluded if artifacts were present. Artifacts were produced either by participant movement during imaging, or echo-to-echo phase inconsistency. An example quantitative susceptibility map from a study participant with SPMS is shown in Fig. 1.

2.5. Statistical analysis

Cross-sectional analyses were performed using baseline participant data obtained at entry into the MS-STAT2 trial. Associations were assessed using multivariable linear regression. Age and sex were included as covariates in all models. For analyses between participant groups, ROI susceptibility was the dependent variable, and patient group (SPMS or control) the predictor. Only when deep grey matter nuclei susceptibility was significantly different between patients and controls were the associations between MS severity variables and ROI susceptibility then examined. To assess the degree to which changes in ROI susceptibility were associated with clinical or imaging measures of MS severity, in such models, ROI susceptibility was used as the predictor, with the clinical or imaging measure of MS severity as the dependent variable, again adjusting for age and sex. To determine the extent to which such relationships between ROI susceptibility and clinical disability were independent of established imaging measures of disease severity, such models were then repeated whilst including T2LV and ROI normalised volume as covariates. Due to violation of regression model assumptions (residuals not normally distributed on visual inspection of histograms and QQ plots, or clear heteroskedasticity visible on visual inspection of residual-versus-fitted plots), models with EDSS or SLVCA as the dependent variable were based upon bias-corrected and accelerated bootstrap with 10,000 replications. P-values are therefore not directly calculated, but may be inferred from the 95% and 99% confidence intervals (whereby if the 95% CI does not include no effect, the inferred p-value <0.05; if the 99% CI does not include no effect, the inferred p-value <0.01.)

3. Results

3.1. Cohort characteristics

Characteristics of the included cohort are shown in Table 1. Participants had features typical of established SPMS, with a prolonged disease duration, substantial physical disability, high T2LV and a low degree of inflammatory disease activity at baseline. No participants were receiving immunomodulatory disease modifying therapy at the time of imaging or within the preceding 6 months.

As expected, patients with MS had significantly lower brain volumes and higher T2 lesion volumes compared to controls (all p < 0.05). Compared to patients, controls were also significantly older (57 vs. 53 years, p = 0.006), and less likely to be female (52% vs. 77%, p = 0.004). In both patients and controls, thalamic susceptibility tended to decrease
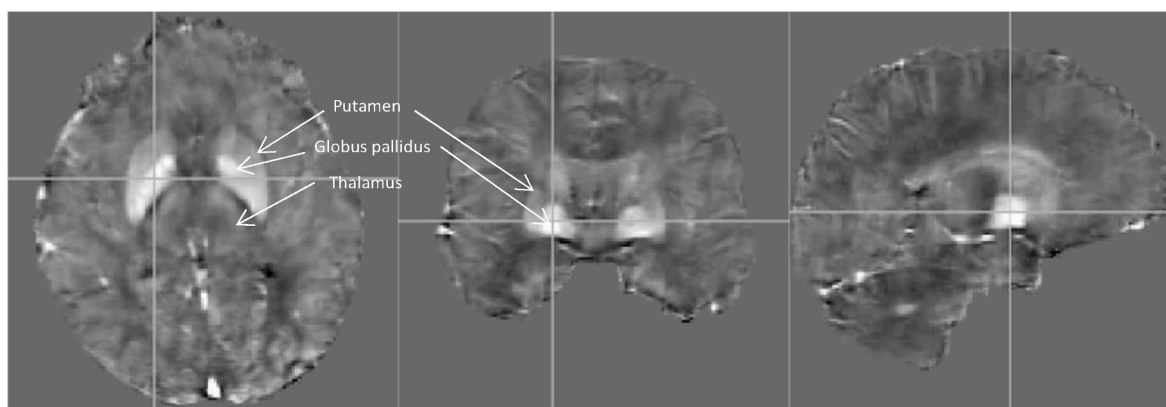
Fig. 1. Example quantitative susceptibility map (QSM) from a study participant with secondary progressive multiple sclerosis. Left to right: axial, coronal and sagittal planes. Images are presented at the level of the basal ganglia to demonstrate the high susceptibility seen in the globus pallidus and putamen. The greyscale represents voxel susceptibility, which across the whole brain ranges from −225 (black) to +300 (white) ppb.

Table 1
Characteristics of the study cohort following exclusions.

	SPMS	Control
N	149	33
Age (mean, SD)	53.4 (7.2)	57.3 (6.7)
Female (%)	77%	52%
Disease duration (years, mean SD)	23.8 (9.5)	–
EDSS (median, IQR)	6 (4.5–6.0)	–
nWBV (mL, mean SD)	1430.7 (69.5)	1464.2 (67.2)
Thalamic volume (mL, mean, SD)	11.3 (1.5)	13.1 (1.2)
Putamen volume (mL, mean, SD)	9.6 (1.3)	10.8 (1.2)
Globus pallidus volume (mL, mean, SD)	1.6 (0.2)	1.7 (0.2)
T2LV (mL, median, IQR)	20.7 (12.2–36.3)	3.0 (1.9–5.7)
T1-GAD + lesions	11.3%	–
N excluded (%)[a]	16 (9.7%)	5 (13.5%)

[a] Number of participants excluded following a visual inspection of QSM images. SD, standard deviation; IQR, interquartile range; nWBV, normalised whole brain volume; T2LV, T2 lesion volume; T1-GAD+, T1 post-gadolinium enhancing lesions.

with older age, and susceptibility in the putamen was slightly lower in females (Table S1). Both age and sex were therefore included as covariates in all subsequent analyses.

3.2. Deep grey matter regional susceptibility in patients and controls

Unadjusted regional susceptibility between patients and controls are shown in Fig. 2. Beta-coefficients, with adjustment for age and sex, are shown in Table 2. In the globus pallidus and putamen, susceptibility was similar between patients and controls. There was, however, strong evidence to support thalamic susceptibility being lower in pwSPMS (unadjusted mean: 28.6 (SD 12.8) ppb) compared to controls (39.2 (SD 12.7) ppb). After adjusting for age and sex, modelled thalamic susceptibility was 12.0 ppb lower in people with SPMS (95% CI −17.0 to −7.1, $p < 0.001$).

3.3. Thalamic susceptibility and MS clinical severity variables

As thalamic susceptibility was significantly different in SPMS compared to controls, the relationships between thalamic susceptibility and MS clinical severity variables were investigated (Table 3). In
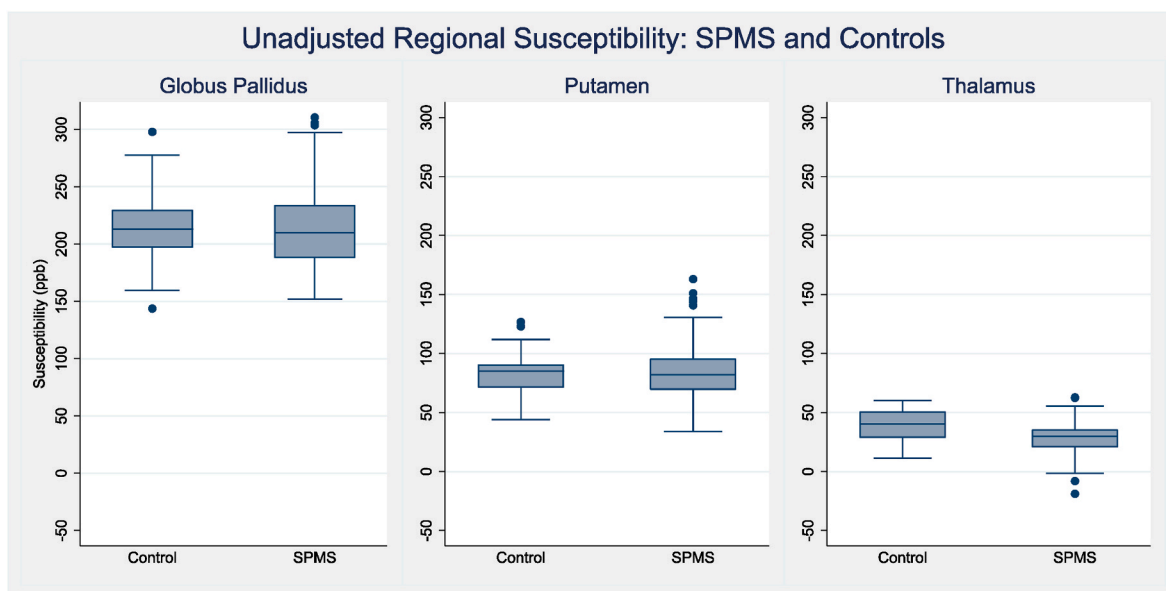

Fig. 2. Deep grey matter regional susceptibility: SPMS vs. Controls. Unadjusted box-plots showing ROI susceptibility (ppb) between patients and controls. SPMS, secondary progressive multiple sclerosis; ROI, region of interest; ppb, parts per billion.

Table 2

Comparison of deep grey matter susceptibility between patients and controls.

	Beta-coefficient [95% CI] SPMS, relative to controls
Globus pallidus susceptibility (ppb)	1.26 [-12.6 to +15.2] p = 0.859
Putamen susceptibility (ppb)	2.33 [-6.3 to +11.0] p = 0.597
Thalamus susceptibility (ppb)	−12.0 [-17.0 to −7.1] p < 0.001

The results were derived from 3 separate multivariable linear regression models. Regional susceptibility was the dependent variable, with SPMS/control status (SPMS = 1, control = 0) as the independent variable. Age and sex were included as covariates. Susceptibility was expressed as ppb. The coefficients therefore relate to the difference in ROI susceptibility for pwSPMS, relative to controls. CI, confidence interval; ppb, parts per billion; SPMS, secondary progressive multiple sclerosis.

Table 3

Association between thalamic susceptibility and clinical MS severity variables.

Clinical Variable	Beta-coefficient [95% CI] thalamic susceptibility
EDSS (score)	−0.013 [−0.024 to −0.001] p<0.05*
25FW_speed (ft/1000s)	+6.71 [−8.83 to 22.27] p = 0.395
9HPT_speed_dom (1/1000s)	+0.03 [−0.11 to +0.17] p = 0.691
9HPT_speed_nondom (1/1000s)	+0.05 [−0.09 to +0.19] p = 0.450
SDMT (score)	+0.24 [+0.10 to +0.38] p = 0.001
CVLT-II (score)	+0.14 [−0.00 to +0.29] p = 0.058
BVMT-R (score)	+0.10 [−0.00 to +0.21] p = 0.053
SLCVA 2.5% (score)	+0.24 [+0.11 to +0.37] P<0.01*
SLCVA 1.25% (score)	+0.19 [+0.07 to +0.30] p<0.01*

The results were derived from 9 separate multivariable linear regression models. Clinical disability measures were the dependent variable, and ROI susceptibility the predictor. Age and sex were included as covariates in all analyses, and for the cognitive variables (SDMT, CVLT-II and BVMT-R) years in education was included as an additional covariate. Susceptibility is expressed as ppb. * Signifies that in these models, due to violation of regression model assumptions, models were based upon bias-corrected and accelerated bootstrap with 10,000 replications. P-values are therefore not directly calculated, but may be inferred from the 95% (and where required, 99%) confidence intervals. If the 95% CI does not include no effect, the inferred p-value <0.05; if the 99% CI does not include no effect, the inferred p-value <0.01. Significant associations (p < or = 0.05) are shown in bold. CI, confidence interval; EDSS, Expanded Disability Status Scale; 25FW, timed 25 foot walk; 9HPT, timed 9-hole peg test; SDMT, symbol digit modalities test; CVLT-II, California verbal learning test; BVMT-R, brief visual memory test; SLCLA 2.5%, Sloan low contrast letter acuity 2.5%; SLCLA 1.25%, Sloan low contrast letter acuity 1.25%.

patients, there was a relationship between *lower* thalamic susceptibility and higher EDSS, poorer SDMT performance and poorer low contrast visual acuity, when adjusting for sex and age. Trends were also present between lower thalamic susceptibility and longer disease duration (Table S2) and poorer working memory performance (CVLT-II and BVMT-R).

3.4. Thalamic susceptibility and MS imaging severity variables

The relationships between thalamic susceptibility and MS imaging severity variables are shown in Table 4. In patients with SPMS, lower thalamic susceptibility was strongly associated with higher T2LV and more severe atrophy of the whole brain, deep grey matter and thalamus.

3.5. Relationships between thalamic susceptibility and MS clinical severity variables after adjustment for MRI derived measures of MS severity

To assess the extent to which the observed significant relationships between thalamic susceptibility and MS clinical severity variables (EDSS, SDMT, SLCVA at 2.5% and 1.25%) persisted independent of

Table 4

Association between thalamic susceptibility and MRI derived measures of MS severity.

Imaging variable	Beta-coefficient [95% CI] thalamic susceptibility
T2LV (mL)	−0.62 [-0.82 to -0.43] p<0.001
nWBV (mL)	+1.56 [+0.71 to +2.41] p<0.001
nDGMV (mL)	+0.10 [+0.05 to +0.14] p<0.001
nThalamic volume (mL)	+0.03 [+0.02 to +0.05] p<0.001

The results were derived from 4 separate multivariable linear regression models. T2LV, nWBV, nDGMV or thalamic volume was the dependent variable (all in mL), and ROI susceptibility the predictor (ppb). Age and sex were included as covariates in all analyses. Significant p values are shown in bold. CI, confidence interval; T2LV, T2 lesion volume; nWBV, normalised whole brain volume; nDGMV, normalised deep grey matter volume; nThalamic volume, normalised thalamic volume.

conventional imaging variables (T2LV, normalised thalamic volume, nWBV), the models were repeated. T2LV, normalised thalamic volume, and normalised whole brain volume were first separately included as additional covariates, followed by a final model including all 3 imaging variables as covariates (Table S3).

When adjusting for T2LV, significant relationships persisted between lower thalamic susceptibility and higher EDSS (beta coefficient: 0.014 [−0.026 to −0.000] EDSS, p < 0.05). When adjusting for normalised thalamic volume, significant relationships persisted between lower thalamic susceptibility and poorer low contrast visual acuity (SLCVA 2.5%; +0.162 [+0.020 to +0.299], p < 0.05). When adjusting for normalised whole brain volume, significant relationships persisted between thalamic susceptibility and poorer SDMT performance (+0.172 [+0.028 to +0.316], p = 0.019); and poorer low contrast visual acuity (SLVCA 2.5%: +0.207 [+0.065 to +0.341], p < 0.01*; SLVCA 1.25%: +0.155 [+0.064 to +0.015], p < 0.05). No significant relationships, however, persisted between thalamic susceptibility and clinical variables when models were simultaneously adjusted for T2LV, normalised thalamic volume and normalised whole brain volume.

Re-assessing the difference in thalamic susceptibility between patients and controls, after adjusting for thalamic normalised volume, thalamic susceptibility remained lower in pwSPMS. A significant interaction term was also present between patient group and thalamic volume, suggesting a stronger relationship is present between thalamic normalised volume and thalamic susceptibility in pwSPMS compared to controls (Table S4).

4. Discussion

We have examined cross-sectional regional QSM-derived susceptibility data in a large SPMS population with an age-matched control cohort. Our analysis was restricted to ROI within the deep grey matter, as QSM-derived susceptibility has only been sufficiently validated as a measure of iron concentration within these structures. The key finding is that lower thalamic susceptibility is present in SPMS and associated with more severe disease across a number of domains. In contrast to the existing literature, we found globus pallidus and putamen susceptibility to be similar between patients and controls.

4.1. Thalamic susceptibility

Our results and the existing literature suggests that thalamic susceptibility may correlate with important pathogenic mechanisms of multiple sclerosis disease progression. Thalamic susceptibility demonstrated strong relationships with T2LV and thalamic atrophy. The relationship between thalamic susceptibility and thalamic atrophy appeared to be an MS-specific effect, as a significant interaction was present between thalamic volume and patient group, and no relationship was apparent when controls were examined in isolation. The relationship between T2LV and thalamic susceptibility was particularly strong

(univariable R^2 = 19.3%), although a significant relationship between higher EDSS and lower thalamic susceptibility persisted after adjusting for T2LV. Lower thalamic susceptibility may therefore be a promising imaging biomarker of disease severity in progressive MS.

Lower thalamic susceptibility may potentially be caused by lower iron concentrations or increases in the density of diamagnetic substances, such as myelin or calcium. Given the absence of evidence regarding thalamic calcium accumulation, increased myelin density or lower iron concentrations should be considered (Schweser et al., 2018). We now consider these in turn.

In progressive MS, demyelination has been reported to be common in the thalamus, more so than in the globus pallidus or putamen (Haider et al., 2014; Vercellino et al., 2009). The median percentage area of thalamic histological slides showing demyelination was 7.4% (IQR 2.2%–17.1%) in those with progressive MS (Haider et al., 2014). Whilst demyelination is therefore relatively common in the thalamus, demyelination in isolation would be expected to cause increases in susceptibility. This is the opposite of what we have observed and therefore demyelination alone is unlikely to be the predominant mechanism of thalamic susceptibility changes.

As for iron, the principal sites of storage within the deep grey matter, as for elsewhere within the CNS, has been reported to be oligodendrocytes and myelin, and to a lesser extent neurones, astrocytes and microglia (Haider et al., 2014). A reduction in the density of these structures, as has previously been reported to occur in a cohort of predominantly SPMS, may therefore lead to a loss of such iron stores from the thalamus, and hence reduced susceptibility (Mahajan et al., 2020). The thalamus has a higher myelin density than other deep grey matter structures, which may explain why changes in thalamic susceptibility demonstrate a similar pattern to white matter lesions (chronically demyelinated lesions typically have a reduced susceptibility), in contrast to the structures of the basal ganglia (Hametner et al., 2018). Reduced thalamic iron as the principal cause of reduced thalamic susceptibility is also supported by observations from studies using combined QSM and R2* imaging. As both QSM-derived susceptibility and R2* signal are positively correlated with iron concentration, but demonstrate the opposite relationships with myelin density, the positive correlation between thalamic susceptibility and R2* signal suggests thalamic iron is the predominant determinant of both the thalamic susceptibility and R2* signal (Schweser et al., 2018; Fujiwara et al., 2017).

As to the cause of such pathological changes within the thalamus, combined histological and imaging studies have suggested that they are driven by extra-thalamic processes. Lower thalamic volume was associated with lower thalamic neuronal density, higher global T1 and T2 lesion volumes, and lower normalised whole brain and cortical volumes. In contrast, thalamic volume was not associated with the volume of thalamic demyelinating lesions (Mahajan et al., 2020). It therefore appears that extra-thalamic pathological processes are the most significant contributors to atrophy and neuroaxonal loss within the thalamus. This is likely mediated via Wallerian degeneration along the many thalamo-cortical tracts disrupted by white matter or cortical lesions (Mahajan et al., 2020). The extensive connectivity of the thalamus with multiple cortical and subcortical areas likely contributes to its vulnerability to such secondary neurodegenerative effects (Kumar et al., 2017; Papadopoulou et al., 2019). The impact of these extra-thalamic processes upon the thalamus itself may then result in reduced thalamic susceptibility through the resulting degeneration of oligodendrocytes and axons due to the loss of their contained iron stores.

This pathological sequence of events is supported by our findings that thalamic susceptibility is strongly associated with both T2LV and thalamic normalised volume. As the reduction in thalamic susceptibility would be expected to occur concurrently with, and of a similar magnitude to, the reduction in thalamic volume, it is therefore logical that the associations we observed between thalamic susceptibility and measures of MS clinical severity were reduced after inclusion of thalamic normalised volume as a covariate.

4.2. Globus pallidus and putamen susceptibility

We did not find significant increases in the mean regional susceptibility of either the putamen or globus pallidus compared to controls. This contrasts with the previous literature, where increased susceptibility has been reported in these structures (Hagemeier et al., 2018a, 2018b; Zivadinov et al., 2018; Voon et al., 2024). This may relate to the older age of our recruited cohort.

Prior studies that have reported higher susceptibility within the globus pallidus or putamen compared to controls generally included younger participants compared to our cohort (see Table S4; mean ages of previous cohorts 44–50 years, compared to 53 in our cohort). Basal ganglia susceptibility is known to display a non-linear increase with age in healthy controls (Hallgren and Sourander, 1958). In histological studies, deep grey matter [iron] was shown to increase with age in healthy controls, but not in pwMS (Haider et al., 2014). Additionally, higher basal ganglia susceptibility has been demonstrated from the earliest clinical stages of MS, and in longitudinal studies, the rate of increase in basal ganglia susceptibility may be greater in the earlier stages of MS compared to those with longer disease duration (Hagemeier et al., 2018b; Schweser et al., 2020; Khalil et al., 2015; Langkammer et al., 2013). Taken together, these reports therefore suggest that our older cohort may be responsible for the similar susceptibility in the globus pallidus and putamen between patients and controls, due to the ongoing age-related increases in susceptibility seen in controls. The ages of patients and controls in our study were also not perfectly matched (SPMS: 53; controls: 57). Whilst age was included as a covariate in all analyses, we cannot exclude the slightly older age of the controls also contributing to our results. One possible interpretation of our data from the basal ganglia, in the context of the existing literature, is therefore that increased susceptibility in the basal ganglia may occur early in MS and is associated with a more severe disease course, as reported in previous studies (Hagemeier et al., 2018a, 2018b; Zivadinov et al., 2018). As previously discussed, this increased susceptibility may principally reflect increased iron concentrations secondary to structural atrophy, rather than an increased iron content (Hagemeier et al., 2018b; Schweser et al., 2020). By the advanced age of our cohort, however, a plateauing of basal ganglia susceptibility in patients, combined with ongoing age-related increases in basal ganglia susceptibility in controls, results in similar cross-sectional regional susceptibility values.

This study is not without limitations. The above interpretations are speculative and limited by the cross-sectional design. Follow-up of this cohort is ongoing, and future longitudinal analyses are likely to provide further insights into the role of DGM susceptibility as a biomarker in SPMS. Additionally, although QSM-derived susceptibility has been validated against deep grey matter iron concentrations, it may still be influenced by other tissue properties such as myelin. Improved quantification of CNS iron, and greater validity outside of the deep grey matter, may therefore be achieved through refinements of the QSM technique that allow separation of the diamagnetic and paramagnetic contributions of myelin and iron. This can be achieved through inclusion of both phase and magnitude data, and may improve specificity to tissue myelin and iron content (Emmerich et al., 2021).

4.3. Conclusions

Lower thalamic susceptibility is present in people with SPMS compared to controls and associated with a number of clinical and imaging measures of MS severity. Different regional and temporal perturbations in iron handling appear important in the pathophysiology of progressive MS, encouraging further investigation and development of QSM imaging as a biomarker of disease progression.

Disclosures

CRediT authorship contribution statement

Thomas Williams: Writing – review & editing, Writing – original draft, Investigation, Formal analysis, Data curation, Conceptualization. **Nevin John:** Writing – review & editing, Investigation, Data curation. **Alberto Calvi:** Writing – review & editing, Investigation, Data curation. **Alessia Bianchi:** Writing – review & editing, Investigation, Data curation. **Floriana De Angelis:** Writing – review & editing, Investigation, Data curation. **Anisha Doshi:** Writing – review & editing, Investigation, Data curation. **Sarah Wright:** Writing – review & editing, Investigation, Data curation. **Madiha Shatila:** Writing – review & editing, Investigation, Data curation. **Marios C. Yiannakas:** Writing – review & editing, Investigation, Data curation. **Fatima Chowdhury:** Writing – review & editing, Data curation. **Jon Stutters:** Writing – review & editing, Investigation, Data curation. **Antonio Ricciardi:** Writing – review & editing, Investigation, Data curation. **Ferran Prados:** Writing – review & editing, Investigation, Data curation. **David MacManus:** Writing – review & editing, Supervision. **Francesco Grussu:** Writing – review & editing, Data curation. **Anita Karsa:** Writing – review & editing, Software, Methodology, Data curation. **Becky Samson:** Writing – review & editing, Methodology, Data curation. **Marco Battiston:** Writing – review & editing, Software, Methodology, Data curation. **Claudia A.M. Gandini Wheeler-Kingshott:** Writing – review & editing, Software, Methodology, Funding acquisition, Data curation. **Karin Shmueli:** Writing – review & editing, Software, Methodology, Data curation, Conceptualization. **Olga Ciccarelli:** Writing – review & editing, Supervision, Funding acquisition. **Frederik Barkhof:** Writing – review & editing, Supervision, Funding acquisition. **Jeremy Chataway:** Writing – review & editing, Supervision, Investigation, Funding acquisition, Data curation, Conceptualization.

Declaration of competing interest

The authors declare that they have no known competing financial interests or personal relationships that could have appeared to influence the work reported in this paper.

Data availability

The data that has been used is confidential.

Appendix A. Supplementary data

Supplementary data to this article can be found online at https://doi.org/10.1016/j.ynirp.2024.100216.

References

Bilgic, B., Langkammer, C., Marques, J.P., Meineke, J., Milovic, C., Schweser, F., 2021. QSM reconstruction challenge 2.0: design and report of results. Magn. Reson. Med. 86 (3), 1241–1255.

Buckner, R.L., Head, D., Parker, J., Fotenos, A.F., Marcus, D., Morris, J.C., et al., 2004. A unified approach for morphometric and functional data analysis in young, old, and demented adults using automated atlas-based head size normalization: reliability and validation against manual measurement of total intracranial volume. Neuroimage 23 (2), 724–738.

Bulters, D., Gaastra, B., Zolnourian, A., Alexander, S., Ren, D., Blackburn, S.L., et al., 2018. Haemoglobin scavenging in intracranial bleeding: biology and clinical implications. Nat. Rev. Neurol. 14 (7), 416–432. https://doi.org/10.1038/s41582-018-0020-0 [Internet].

Cardoso, M.J., Modat, M., Wolz, R., Melbourne, A., Cash, D., Rueckert, D., et al., 2015. Geodesic information Flows: spatially-variant graphs and their application to segmentation and fusion. IEEE Trans. Med. Imag. 34 (9), 1976–1988.

Cornell MRI Research Lab, 2020. Quantitative Susceptibility Mapping MEDI Toolbox [Internet]. Available from: https://pre.weill.cornell.edu/mri/pages/qsm.html. (Accessed 27 February 2024).

Emmerich, J., Bachert, P., Ladd, M.E., Straub, S., 2021. On the separation of susceptibility sources in quantitative susceptibility mapping: theory and phantom validation with an in vivo application to multiple sclerosis lesions of different age. J. Magn. Reson. 330, 107033 https://doi.org/10.1016/j.jmr.2021.107033 [Internet].

FreeSurfer, 2021. eTIV - Estimated Total Intracranial Volume, Aka ICV [Internet]. Available from: https://surfer.nmr.mgh.harvard.edu/fswiki/eTIV.

Fujiwara, E., Kmech, J.A., Cobzas, D., Sun, H., Seres, P., Blevins, G., et al., 2017. Cognitive implications of deep gray matter iron in multiple sclerosis. Am. J. Neuroradiol. 38 (5), 942–948.

Hagemeier, J., Ramanathan, M., Schweser, F., Dwyer, M.G., Lin, F., Bergsland, N., et al., 2018a. Iron-related gene variants and brain iron in multiple sclerosis and healthy individuals. NeuroImage Clin 17, 530–540.

Hagemeier, J., Zivadinov, R., Dwyer, M.G., Polak, P., Bergsland, N., Weinstock-Guttman, B., et al., 2018b. Changes of deep gray matter magnetic susceptibility over 2 years in multiple sclerosis and healthy control brain. NeuroImage Clin 18 (December 2016), 1007–1016. https://doi.org/10.1016/j.nicl.2017.04.008 [Internet].

Hagemeier, J., Zivadinov, R., Dwyer, M.G., Polak, P., Bergsland, N., Weinstock-Guttman, B., et al., 2018c. Changes of deep gray matter magnetic susceptibility over 2 years in multiple sclerosis and healthy control brain - supplement. NeuroImage Clin 18, 1007–1016.

Haider, L., Simeonidou, C., Steinberger, G., Hametner, S., Grigoriadis, N., Deretzi, G., et al., 2014. Multiple sclerosis deep grey matter: the relation between demyelination, neurodegeneration, inflammation and iron. J. Neurol. Neurosurg. Psychiatry 85 (12), 1386–1395.

Hametner, S., Wimmer, I., Haider, L., Pfeifenbring, S., Brück, W., Lassmann, H., 2013. Iron and neurodegeneration in the multiple sclerosis brain. Ann. Neurol. 74 (6), 848–861.

Hallgren, B., Sourander, P., 1958. The effect of age on the non-haemin iron in the human brain. J. Neurochem. 3 (1), 41–51.

Hametner, S., Endmayr, V., Deistung, A., Palmrich, P., Prihoda, M., Haimburger, E., et al., 2018. The influence of brain iron and myelin on magnetic susceptibility and effective transverse relaxation - a biochemical and histological validation study. Neuroimage 179 (May), 117–133.

Karsa, A., Punwani, S., Shmueli, K., 2020. An optimized and highly repeatable MRI acquisition and processing pipeline for quantitative susceptibility mapping in the head-and-neck region. Magn. Reson. Med. 84 (6), 3206–3222.

Khalil, M., Langkammer, C., Pichler, A., Pinter, D., Gattringer, T., Bachmaier, G., et al., 2015. Dynamics of brain iron levels in multiple sclerosis. Neurology 84 (1), 1–8.

Kiersnowski, O.C., Karsa, A., Wastling, S.J., Thornton, J.S., Shmueli, K., 2023. Investigating the effect of oblique image acquisition on the accuracy of QSM and a robust tilt correction method. Magn. Reson. Med. 89 (5), 1791–1808.

Kumar, V.J., van Oort, E., Scheffler, K., Beckmann, C.F., Grodd, W., 2017. Functional anatomy of the human thalamus at rest. Neuroimage 147 (October 2016), 678–691.

Langkammer, C., Schweser, F., Krebs, N., Deistung, A., Goessler, W., Scheurer, E., et al., 2012. Quantitative susceptibility mapping (QSM) as a means to measure brain iron? A post mortem validation study. Neuroimage 62 (3), 1593–1599. https://doi.org/10.1016/j.neuroimage.2012.05.049 [Internet].

Langkammer, C., Liu, T., Khalil, M., Enzinger, C., Jehna, M., Fuchs, S., et al., 2013. Quantitative susceptibility mapping in multiple sclerosis. Radiology 267 (2), 551–559.

Liu, T., Khalidov, I., de Rochefort, L., Spincemaille, P., Liu, J., Tsiouris, A.J., et al., 2011. A novel background field removal method for MRI using projection onto dipole fields (PDF). NMR Biomed. 24 (9), 1129–1136.

Liu, T., Wisnieff, C., Lou, M., Chen, W., Spincemaille, P., Wang, Y., 2013. Nonlinear formulation of the magnetic field to source relationship for robust quantitative susceptibility mapping. Magn. Reson. Med. 69 (2), 467–476.

Mahajan, K.R., Nakamura, K., Cohen, J.A., Trapp, B.D., Ontaneda, D., 2020. Intrinsic and extrinsic mechanisms of thalamic pathology in multiple sclerosis. Ann. Neurol. 88 (1), 81–92.

Mehta, V., Pei, W., Yang, G., Li, S., Swamy, E., Boster, A., et al., 2013. Iron is a sensitive biomarker for inflammation in multiple sclerosis lesions. PLoS One 8 (3), 1–10.

Murdoch, R., Stotesbury, H., Kawadler, J.M., Saunders, D.E., Kirkham, F.J., Shmueli, K., 2022. Quantitative susceptibility mapping (QSM) and R2* of silent cerebral infarcts in sickle cell anemia. Front. Neurol. 13.

Papadopoulou, A., Gaetano, L., Pfister, A., Altermatt, A., Tsagkas, C., Morency, F., et al., 2019. Damage of the lateral geniculate nucleus in MS: assessing the missing node of the visual pathway. Neurology 92 (19), E2240–E2249.

Popescu, B.F., Frischer, J.M., Webb, S.M., Tham, M., Adiele, R.C., Robinson, C.A., et al., 2017. Pathogenic implications of distinct patterns of iron and zinc in chronic MS lesions. Acta Neuropathol. 134 (1), 45–64.

Ricciardi, A., Karsa, A., Tur, C., Calvi, A., Collorone, S., Grussu, F., et al., 2021. The effect of echo train length and TE range on multi-echo quantitative susceptibility mapping. ISMRN (Figure 3), 6–9.

Sastre-Garriga, J., Pareto, D., Battaglini, M., Rocca, M.A., Ciccarelli, O., Enzinger, C., et al., 2020. MAGNIMS consensus recommendations on the use of brain and spinal cord atrophy measures in clinical practice. Nat. Rev. Neurol. 16 (3), 171–182. https://doi.org/10.1038/s41582-020-0314-x [Internet].

Schweser, F., Deistung, A., Sommer, K., Reichenbach, J.R., 2013. Toward online reconstruction of quantitative susceptibility maps: superfast dipole inversion. Magn. Reson. Med. 69 (6), 1581–1593.

Schweser, F., Raffaini Duarte Martins, A.L., Hagemeier, J., Lin, F., Hanspach, J., Weinstock-Guttman, B., et al., 2018. Mapping of thalamic magnetic susceptibility in multiple sclerosis indicates decreasing iron with disease duration: a proposed mechanistic relationship between inflammation and oligodendrocyte vitality. Neuroimage 167 (July 2017), 438–452. https://doi.org/10.1016/j.neuroimage.2017.10.063 [Internet].

Schweser, F., Hagemeier, J., Dwyer, M.G., Bergsland, N., Hametner, S., Weinstock-Guttman, B., et al., 2020. Decreasing brain iron in multiple sclerosis: the difference between concentration and content in iron MRI. Hum. Brain Mapp. 42 (5), 1463–1474.

Shmueli, K., De Zwart, J.A., Van Gelderen, P., Li, T.Q., Dodd, S.J., Duyn, J.H., 2009. Magnetic susceptibility mapping of brain tissue in vivo using MRI phase data. Magn. Reson. Med. 62 (6), 1510–1522.

Stüber, C., Morawski, M., Schäfer, A., Labadie, C., Wähnert, M., Leuze, C., et al., 2014. Myelin and iron concentration in the human brain: a quantitative study of MRI contrast. Neuroimage 93 (P1), 95–106. https://doi.org/10.1016/j.neuroimage.2014.02.026 [Internet].

Sun, H., Walsh, A.J., Lebel, R.M., Blevins, G., Catz, I., Lu, J.-Q., et al., 2015. Validation of quantitative susceptibility mapping with Perls' iron staining for subcortical gray matter. Neuroimage 105, 486–492.

Tham, M., Frischer, J.M., Weigand, S.D., Fitz-Gibbon, P.D., Webb, S.M., Guo, Y., et al., 2020. Iron heterogeneity in early active multiple sclerosis lesions. Ann. Neurol. 1–13.

Todorich, B., Pasquini, J.M., Garcia, C.I., Paez, P.M., Connor, J.R., 2009. Oligodendrocytes and myelination: the role of iron. Glia 57 (5), 467–478.

Valverde, S., Salem, M., Cabezas, M., Pareto, D., Vilanova, J.C., Ramió-Torrentà, L., et al., 2019. One-shot domain adaptation in multiple sclerosis lesion segmentation using convolutional neural networks. NeuroImage Clin 21, 101638.

Vercellino, M., Masera, S., Lorenzatti, M., Condello, C., Merola, A., Mattioda, A., et al., 2009. Demyelination, inflammation, and neurodegeneration in multiple sclerosis deep gray matter. J. Neuropathol. Exp. Neurol. 68 (5), 489–502.

Voon, C.C., Wiltgen, T., Wiestler, B., Schlaeger, S., Mühlau, M., 2024. Quantitative susceptibility mapping in multiple sclerosis: a systematic review and meta-analysis. NeuroImage Clin 42 (December 2023), 103598. https://doi.org/10.1016/j.nicl.2024.103598 [Internet].

World Medical Association. Declaration of Helsinki: ethical principles for medical research involving human subjects. (http://www.wma.net/en/30publications/10policies/b3/17c.pdf).

Yong, H.Y.F., Yong, V.W., 2022. Mechanism-based criteria to improve therapeutic outcomes in progressive multiple sclerosis. Nat. Rev. Neurol. 18 (1), 40–55.

Zivadinov, R., Tavazzi, E., Bergsland, N., Hagemeier, J., Lin, F., Dwyer, M.G., et al., 2018. Brain iron at quantitative MRI is associated with disability in multiple sclerosis. Radiology 289 (2), 487–496.

Further reading

Elkady, A.M., Cobzas, D., Sun, H., Blevins, G., Wilman, A.H., 2017. Progressive iron accumulation across multiple sclerosis phenotypes revealed by sparse classification of deep gray matter. J. Magn. Reson. Imag. 46 (5), 1464–1473.